



Article

Correlation Between Composition and Electrodynamics Properties in Nanocomposites Based on Hard/Soft Ferrimagnetics with Strong Exchange Coupling

Munirah Abdullah Almessiere ^{1,2} , Alex V. Trukhanov ^{3,4,5,*} , Yassine Slimani ⁶ , K.Y. You ⁷ , Sergei V. Trukhanov ^{3,4,5}, Ekaterina L. Trukhanova ^{3,5}, F. Esa ⁸, A. Sadaqat ⁹, K. Chaudhary ¹⁰, Maxim Zdorovets ^{11,12,13} and Abdulhadi Baykal ²

¹ Department of Physics, College of Science, Institute for Research & Medical Consultations (IRMC), Imam Abdulrahman Bin Faisal University, P.O. Box 1982, 31441 Dammam, Saudi Arabia; malmessiere@iau.edu.sa

² Department of Nano-Medicine Research, Institute for Research & Medical Consultations (IRMC), Imam Abdulrahman Bin Faisal University, P.O. Box 1982, 31441 Dammam, Saudi Arabia; abaykal@iau.edu.sa

³ SSPA “Scientific and practical materials research center of NAS of Belarus”, 220072 Minsk, Belarus; sv_trukhanov@mail.ru (S.V.T.), kastor1986@yandex.ru (E.L.T.)

⁴ South Ural State University, 454080 Chelyabinsk, Russia

⁵ National University of Science and Technology MISiS, 119049 Moscow, Russia

⁶ Department of Physics Research, Institute for Research & Medical Consultations (IRMC), Imam Abdulrahman Bin Faisal University, P.O. Box 1982, 31441 Dammam, Saudi Arabia; yasslimani@iau.edu.sa

⁷ School of Electrical Engineering, Faculty of Engineering, Universiti Teknologi Malaysia, Skudai-Johor 81310, Malaysia; kyyou@fke.utm.my

⁸ Physics and Chemistry Department, Faculty of Applied Sciences and Technology, Universiti Tun Hussein Onn Malaysia, Pagoh-Johor 81310, Malaysia; fahmir@uthm.edu.my

⁹ Mechanical and Energy Engineering Department, College of Engineering, Imam Abdulrahman Bin Faisal University, P.O. Box 1982, 31441 Dammam, Saudi Arabia; trukhanov86@gmail.com

¹⁰ Physics Department, Faculty of Science, University Teknologi Malaysia, Johor Bahru-Johor 81310, Malaysia; kashif@utm.my

¹¹ L.N. Gumilyov Eurasian National University, Astana 10008, Kazakhstan; m_zdorovets@gmail.com

¹² The Institute of Nuclear Physics of Republic of Kazakhstan, Astana 10008, Kazakhstan

¹³ Ural Federal University named after the First President of Russia B.N. Yeltsin, Yekaterinburg 620002, Russia

* Correspondence: trukhanov86@mail.ru; Tel.: +375-29-518-63-06

Received: 17 January 2019; Accepted: 1 February 2019; Published: 4 February 2019



Abstract: In this work, $\text{Sr}_{0.3}\text{Ba}_{0.4}\text{Pb}_{0.3}\text{Fe}_{12}\text{O}_{19}/(\text{CuFe}_2\text{O}_4)_x$ ($x = 2, 3, 4$, and 5) as strongly exchange-coupled nanosized ferrites were fabricated using a one-pot sol-gel combustion method (citrate sol-gel method). The X-ray diffraction (XRD) powder patterns of the products confirmed the occurrence of pure, exchange-coupled ferrites. Frequency dependencies of the microwave characteristics (MW) were investigated using a co-axial method. The non-linear behavior of the MW with the composition transformation may be due to different degrees of Fe ion oxidation on the spinel/hexaferrite grain boundaries and strong exchange coupling during the hard and soft phases.

Keywords: microwave absorption; nanosized composites; hard-soft ferrites; electromagnetic properties; reflection losses

1. Introduction

Strongly correlated transition metal oxides exhibit a wide spectrum of unusual electronic and magnetic phenomena [1–3] caused by the cooperative effects of charge and spin ordering. This class of materials demonstrates such quantum phenomena as high-temperature superconductivity [4], Bose-Einstein condensation of magnons [5], and multiferroicity (the coexistence of magnetic and ferroelectric ordering) [6]. Functional materials with coexisting hard magnetic and soft magnetic properties at room temperature have attracted much attention [7,8]. The most interesting classes are the multiferroic and electromagnetic composites [9]. The coexistence of two separate magnetic phases may provide strong coupling between them and as a result lead to an improvement of the functional properties [10,11]. For example, it can lead to a modification of the initial electrical and magnetic properties as compared to the pure materials [12]. The main aim is to determine the correlation between chemical compositions (concentration ratio of different phases) and functional properties in composites. The maximal effect in composites can be reached by strong exchange coupling (magnetostatic coupling, intergranular interactions, microstructure effect).

Many researchers have been focused on complex metal oxides based on iron ions (hexaferrites, spinels, perovskites etc.). Barium M-type hexaferrite ($\text{BaFe}_{12}\text{O}_{19}$) and solid solutions based on it are the most attractive objects for investigation. These compounds have a magnetoplumbite structure—space group $P6_3/mmc$ (No. 194) with cell parameters $a = b \approx 5.90 \text{ \AA}$, $c \approx 23.30 \text{ \AA}$. $\text{BaFe}_{12}\text{O}_{19}$ is an important material for microwave applications due to its high saturation magnetization, low electrical conductivity and large magneto-crystalline anisotropy [13]. There are two main mechanisms for microwave absorption in $\text{BaFe}_{12}\text{O}_{19}$: 1. Domain boundary resonance; 2. Natural ferromagnetic resonance. Weakening of the transmitted electromagnetic radiation opens up a wide range of perspectives for microwave absorbers [14–17]. Hard and soft ferrites are technologically important materials owing to their special applications in data-storage media, microwave devices [18] and permanent magnets [19]. Because strong exchange-coupling occurs [20] between two soft and hard magnetic phases, an intensification of the microwave absorption can be observed [21–25]. Shen et al. [26] confirmed the advantages of exchange coupling ferrites.

In this study, $\text{Sr}_{0.3}\text{Ba}_{0.4}\text{Pb}_{0.3}\text{Fe}_{12}\text{O}_{19}/(\text{CuFe}_2\text{O}_4)_x$ ($x = 2, 3, 4$, and 5) composites were produced using a citrate sol-gel method. The correlation between the composition and microwave properties of the composites are discussed.

2. Materials and Methods

$\text{Sr}_{0.3}\text{Ba}_{0.4}\text{Pb}_{0.3}\text{Fe}_{12}\text{O}_{19}/(\text{CuFe}_2\text{O}_4)_x$ ($x = 2, 3, 4$, and 5) composites were produced using a citrate sol-gel method [27–30]. Nitrates of corresponding ions (Fe^{3+} , Ba^{2+} , Pb^{2+} , Cu^{2+}) were mixed to a stoichiometric ratio by adding the citric acid and de-ionized water at a temperature of 355 K. The weight ratio between the citric acid and ion nitrates was 1.5:1. Following that, the mixture was slowly cooled to 298 K. A pH correction using citric acid and a chelation was done. This led to a 3D-structure formation (nitrate-citrate xerogel). Then the xerogel was heated for the “dark gel” phase formation (water evaporation transforms xerogel in the next solution stage—“dark gel” with high viscosity). The “dark gel” was then heated to 523 K by self-ignition. It was accompanied by the formation of a large volume of gas. This first stage allowed us to obtain the initial powders. After pre-firing (at 733 K), samples were calcined at 1373 K for 2 h. The features of the crystal structure and phase compositions were investigated using X-ray diffraction (XRD) under $\text{Cu-K}\alpha$ radiation (Rigaku D/MAX-2400, Japan). The peculiarities of the chemical composition and microstructure were analyzed using Scanning Electron Microscopy (SEM) (Hitachi S-4800, Japan) with Energy-dispersive X-ray spectroscopy (EDX). In addition, we used a high-resolution transmission electron microscopy (HRTEM) (FEI Titan S/TEM microscope, Netherlands). The frequency dependences of the permeability and permittivity were investigated using a co-axial method with an Agilent network analyzer in 8–12 GHz and 100–1000 MHz frequency ranges. The impedance of the co-axial line was normalized ($Z = 50 \text{ Ohm}$).

Based on the obtained values for the real and imaginary parts of the permittivity and permeability (ϵ' , ϵ'' , μ' and μ''), the reflection coefficients were calculated by referring to the theory of propagation of an electromagnetic wave in the transmission line:

$$\dot{R} = \frac{\dot{Z}_M - \dot{Z}}{\dot{Z}_M + \dot{Z}} \quad (1)$$

where, \dot{Z}_M is the impedance of the composite (investigated) material and \dot{Z} is the impedance of the coaxial line (in this case 50 Ohm).

In general, the coaxial line impedance is determined by following equation:

$$\dot{Z} = 60 \ln \left(\frac{D}{d} \right) \sqrt{\frac{\dot{\mu}}{\dot{\epsilon}}} \quad (2)$$

where, D is the outer diameter of the coaxial cable, d is the inner diameter of the coaxial cable, μ is the complex permeability, and ϵ is the complex permittivity.

To calculate reflection losses, the following formulae were used:

$$\dot{R} = \frac{\sqrt{\frac{\dot{\mu}}{\dot{\epsilon}}} - 1}{\sqrt{\frac{\dot{\mu}}{\dot{\epsilon}}} + 1} \quad (3)$$

in dB

$$|\dot{R}| = 20 \lg \left(\frac{\sqrt{\frac{\dot{\mu}}{\dot{\epsilon}}} - 1}{\sqrt{\frac{\dot{\mu}}{\dot{\epsilon}}} + 1} \right) \quad (4)$$

where the modulus of the reflection coefficient shows the ratio of the amplitude of the reflected wave relative to the incident amplitude in dB.

3. Results and Discussion

3.1. Crystal Structure and Microstructure

The XRD patterns of the $\text{Sr}_{0.3}\text{Ba}_{0.4}\text{Pb}_{0.3}\text{Fe}_{12}\text{O}_{19}/(\text{CuFe}_2\text{O}_4)_x$ ($x = 2, 3, 4,$ and 5) samples are presented in Figure 1.

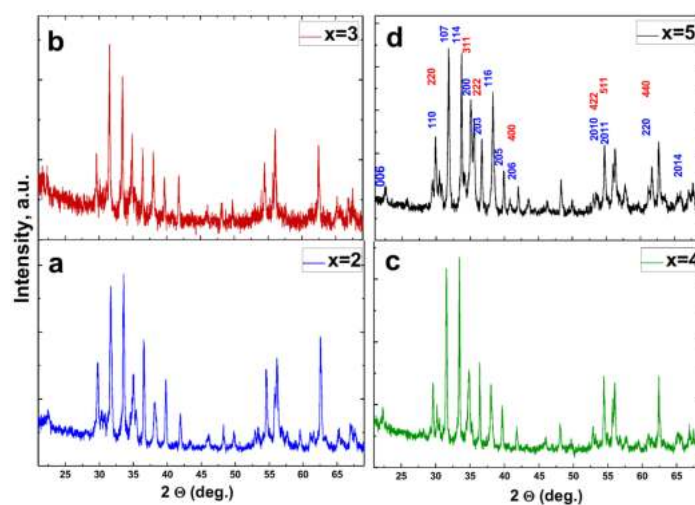


Figure 1. The X-ray diffraction powder patterns of the $\text{Sr}_{0.3}\text{Ba}_{0.4}\text{Pb}_{0.3}\text{Fe}_{12}\text{O}_{19}/(\text{CuFe}_2\text{O}_4)_x$ composite samples $x = 2$ (a), 3 (b), 4 (c), and 5 (d).

The analysis of the XRD data proved the coexistence of two main phases in the samples: CuFe_2O_4 (JCPDS 34-0425) and $\text{BaFe}_{12}\text{O}_{19}$ (JCPDS 00-043-0002). The XRD data was processed using Rietveld Refinement (FullProf. Software). The soft magnetic phase (CuFe_2O_4) corresponds to the spinel structure with Space Group Fd-3m (No. 227)

The hard magnetic phase ($\text{Sr}_{0.3}\text{Ba}_{0.4}\text{Pb}_{0.3}\text{Fe}_{12}\text{O}_{19}$) corresponds to the magneto-plumbite structure with Space Group $P6_3/mmc$ (No. 194). The analysis of the following parameters; R_{wp} (weighted profile R-value), R_{exp} (expected R-value), R_B (Bragg R-factor), R_{mag} (magnetic R-factor) and χ^2 (goodness-of-fit quality factor) was performed after refinement suggested that the investigated samples were of sufficiently good quality and the refinements are effective. The features of the crystal structure for each phase are shown in Table 1.

Table 1. The features of the crystal structure (a and c unit cell parameters and D—average crystallite size) for each phase ($\text{Sr}_{0.3}\text{Ba}_{0.4}\text{Pb}_{0.3}\text{Fe}_{12}\text{O}_{19}$ and CuFe_2O_4) of composites were obtained using XRD data.

Composition	$\text{Sr}_{0.3}\text{Ba}_{0.4}\text{Pb}_{0.3}\text{Fe}_{12}\text{O}_{19}$ hard magnetic phase (Å)		CuFe_2O_4 soft magnetic phase (Å)	D (nm)	
	a	c	a	$\text{Sr}_{0.3}\text{Ba}_{0.4}\text{Pb}_{0.3}\text{Fe}_{12}\text{O}_{19}$	CuFe_2O_4
$\text{Sr}_{0.3}\text{Ba}_{0.4}\text{Pb}_{0.3}\text{Fe}_{12}\text{O}_{19}/(\text{CuFe}_2\text{O}_4)_2$ (1:2)	5.888	23.126	8.411	12.0	32.2
$\text{Sr}_{0.3}\text{Ba}_{0.4}\text{Pb}_{0.3}\text{Fe}_{12}\text{O}_{19}/(\text{CuFe}_2\text{O}_4)_3$ (1:3)	5.880	23.105	8.397	31.8	48.6
$\text{Sr}_{0.3}\text{Ba}_{0.4}\text{Pb}_{0.3}\text{Fe}_{12}\text{O}_{19}/(\text{CuFe}_2\text{O}_4)_4$ (1:4)	5.884	23.104	8.370	25.4	48.3
$\text{Sr}_{0.3}\text{Ba}_{0.4}\text{Pb}_{0.3}\text{Fe}_{12}\text{O}_{19}/(\text{CuFe}_2\text{O}_4)_5$ (1:5)	5.887	23.128	8.323	8.0	38.3

The values of a and c for the hard magnetic phase were slightly varied from 5.880 Å to 5.888 Å and from 23.104 Å to 23.128 Å respectively. The value for the soft magnetic phase was slightly varied from 8.323 Å to 8.411 Å. Negative deviations in unit cell parameters in comparison with bulk ceramics can be explained by the effect of surface compression upon the transition of crystallites to the nano level. For all samples, a structural phase transition was not detected. A phase transition for Cu-spinel from the cubic phase (SG Fd-3m) to the tetragonal phase (sp. gr. I41/amd) was not observed. These results demonstrate to us that the sol-gel method allowed for the growth of both hard and soft ferrites as strongly exchange-coupled composites [18]. This means that there are two separate phases (soft and hard magnetic phases) without chemical interactions with strong magnetostatic coupling (bias exchange between grains) that influences the electromagnetic properties of each phase.

The FE-SEM images and EDX spectra of $\text{Sr}_{0.3}\text{Ba}_{0.4}\text{Pb}_{0.3}\text{Fe}_{12}\text{O}_{19}/(\text{CuFe}_2\text{O}_4)_x$ composite ceramic samples (x = 2, 3, 4, and 5) are presented in Figure 2. The chemical fractions of all elements confirmed the formation of the desired compositions in different samples. The HRTEM images (Figure 3) demonstrate values for distances between the atomic planes of 0.47 and 0.50 nm. This corresponds to the (102) and (100) atomic planes of hexaferrite. Distances between atomic planes of 0.20 nm is typical for the (400) atomic planes of spinels [17,29,30].

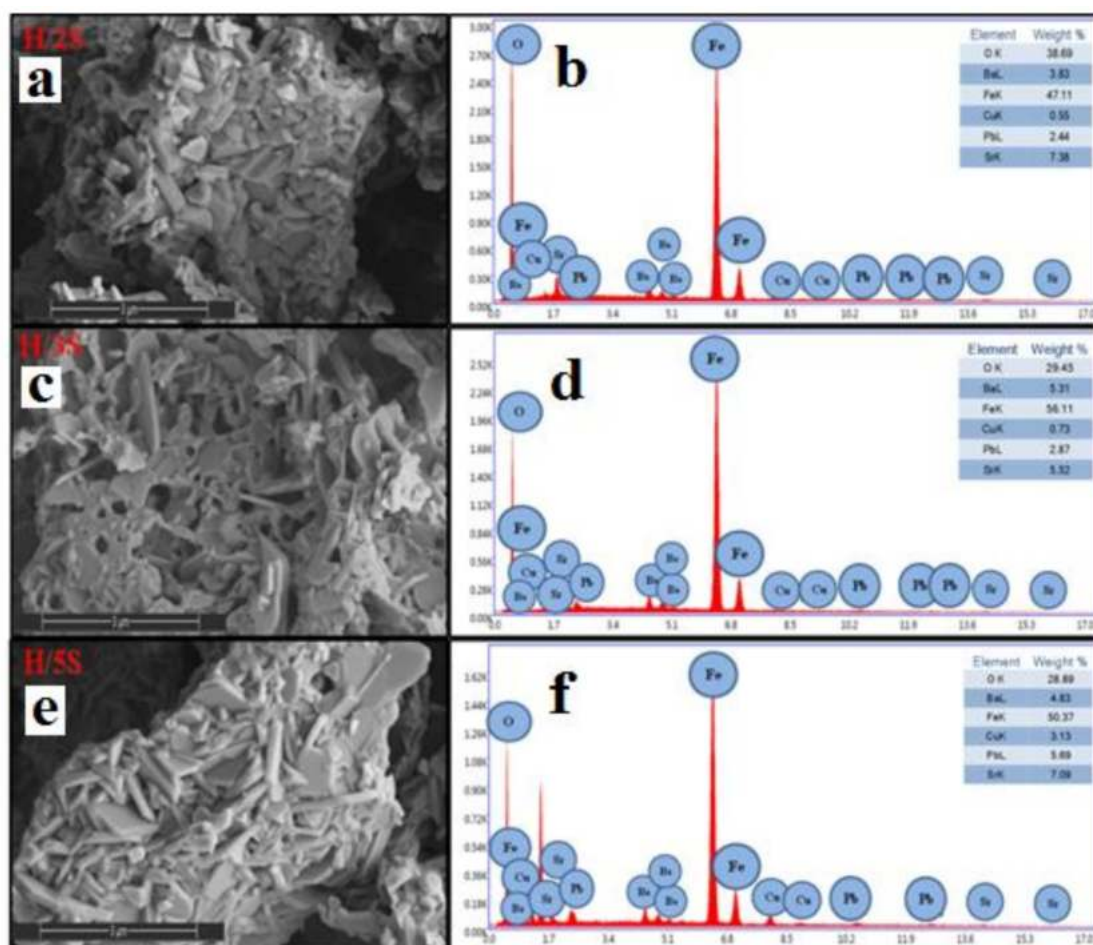


Figure 2. SEM images (a, c, e) and EDX spectra (b, d, f) of $Sr_{0.3}Ba_{0.4}Pb_{0.3}Fe_{12}O_{19}/(CuFe_2O_4)_x$ composite samples $x = 2$ (a, b), 3 (c, d) and 5 (e, f).

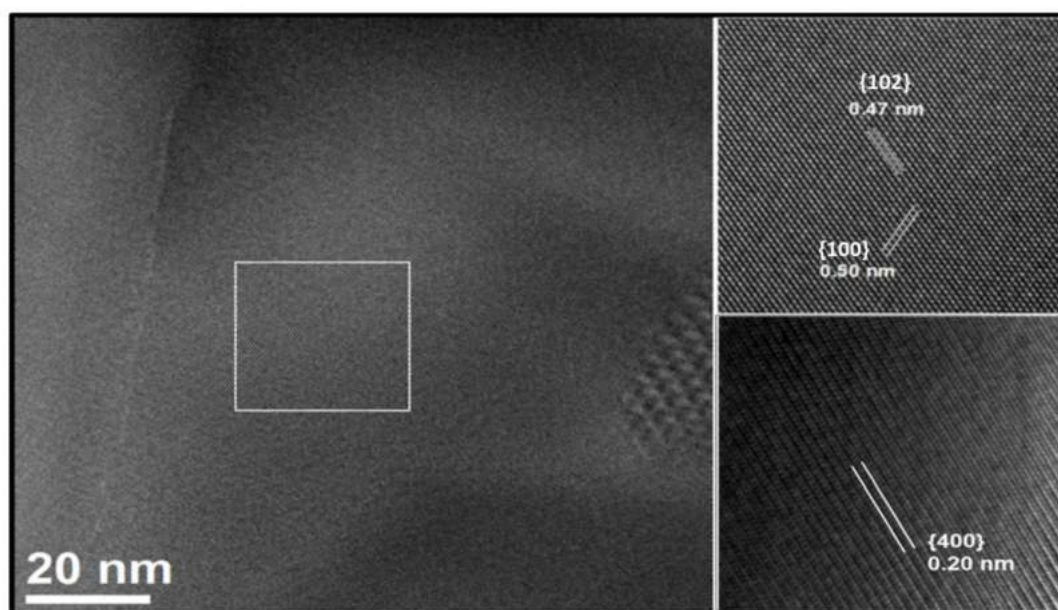


Figure 3. HRTEM images of $Sr_{0.3}Ba_{0.4}Pb_{0.3}Fe_{12}O_{19}/(CuFe_2O_4)_x$ composite samples.

3.2. Electrodynamic Properties

The tangent of the dielectric loss angle ($\text{tg}\delta$), dielectric permittivity (real ϵ' and imaginary ϵ'' parts), magnetic permeability (real μ' and imaginary μ'' parts) and impedance (Z) as functions of frequency were extensively measured by widely adopted coaxial [31,32] and waveguides methods [33–35]. Due to issues related to the measurement dynamical range, the waveguide method is appropriate for narrow frequency ranges only and limited by the size of the sample. Thus, to measure the electrodynamic parameters of the sample in a wide range, it is required to have different measuring sections of the waveguide and to prepare samples of a suitable size.

It is better to use a coaxial or long-line method to measure the electrodynamic parameters of the powder sample in wide-ranging frequencies [36].

Figures 4 and 5 demonstrate frequency dependencies of the permittivity and electrical conductivity. Investigations were carried out at $T = 300$ K in the range of 8–12.5 GHz. Compacted $\text{Sr}_{0.3}\text{Ba}_{0.4}\text{Pb}_{0.3}\text{Fe}_{12}\text{O}_{19}/(\text{CuFe}_2\text{O}_4)_x$ composites ($x = 2, 3, 4,$ and 5) were placed in the co-axial line ($Z = 50$ Ohm). Figure 4 demonstrates that the real (top) and imaginary (bottom) parts of the permittivity depend slightly on frequency.

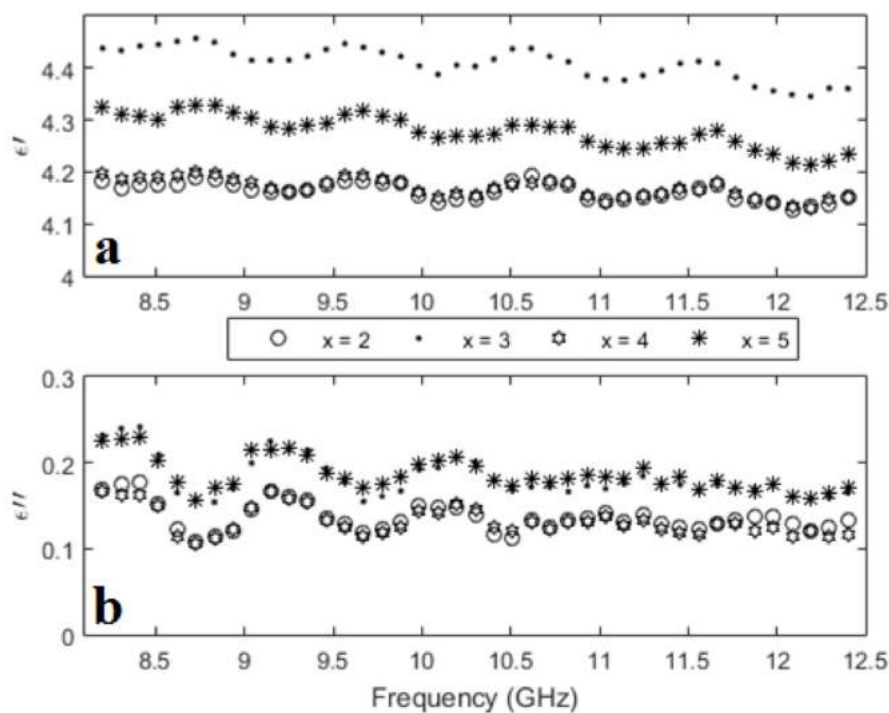


Figure 4. Frequency dependencies of permittivity: real (a) and imaginary (b) parts for $\text{Sr}_{0.3}\text{Ba}_{0.4}\text{Pb}_{0.3}\text{Fe}_{12}\text{O}_{19}/(\text{CuFe}_2\text{O}_4)_x$ composite samples ($x = 2, 3, 4$ and 5).

In the investigated range, no critical changes in permittivity due to the absence of any electrical losses in composites were observed over 8–12.5 GHz. Some blurred peaks on curves (deviation from linearity) can be explained by some insufficient resonance due to geometric factors (interference losses). For the real part, there was an observed dispersion in values for samples with $x = 2, 4$. This non-linear behavior (decrease in permittivity only for samples with a determined concentration without any concentration dependence) may be the result of different degrees of oxidation on the spinel/hexaferrite grain boundaries with a high value of activation energy of conductivity.

Values for the imaginary part of permittivity and active electric conductivity were calculated using the following equations:

$$\epsilon'' = \epsilon' \times \text{tg}\delta \quad (5)$$

$$\sigma_a = \epsilon'' \times \epsilon_0 \omega \quad (6)$$

where, $\text{tg}\delta$ is the loss tangent, σ is the active part of electric conductivity, ϵ_0 is dielectric constant, and ω , is the circular frequency ($2\pi f$).

Figure 5 demonstrates the frequency dependence of the electrical conductivity. The values measured for the conductivity are typical for highly doped semiconductors or composites where realized hopping conduction mechanism occur. The revealed blurred peaks are in agreement with the measurement of permittivity in the same MW range. Differences in conductivity values between compounds with $x = 2$ and 4; $x = 3$ and 5 were determined by the difference in the activation energy of the intergranular potential barrier.

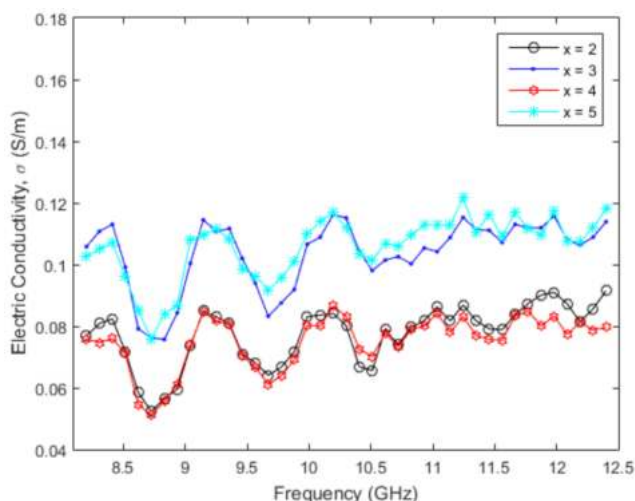


Figure 5. Frequency dependencies of electric conductivity for $\text{Sr}_{0.3}\text{Ba}_{0.4}\text{Pb}_{0.3}\text{Fe}_{12}\text{O}_{19}/(\text{CuFe}_2\text{O}_4)_x$ composite samples ($x = 2, 3, 4$ and 5).

Figure 6 demonstrates the frequency dependence of permeability (real and imaginary parts). Further investigations were carried out at $T = 300$ K in the range 8–12.5 GHz.

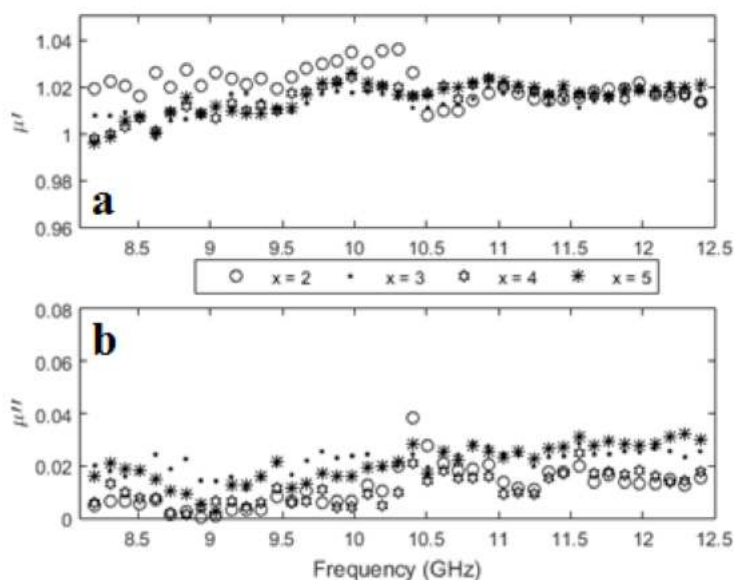


Figure 6. Frequency dependencies of permeability: real (a) and imaginary (b) parts for $\text{Sr}_{0.3}\text{Ba}_{0.4}\text{Pb}_{0.3}\text{Fe}_{12}\text{O}_{19}/(\text{CuFe}_2\text{O}_4)_x$ composite samples ($x = 2, 3, 4$ and 5).

There were no critical changes in permeability due to the absence of any magnetic losses in composites observed in this region. Chemical substitution in hexaferrites must shift the peak of the natural ferromagnetic resonance to the lower frequency region. The calculation of the magnetic

permeability and dielectric permittivity of the $\text{Sr}_{0.3}\text{Ba}_{0.4}\text{Pb}_{0.3}\text{Fe}_{12}\text{O}_{19}/(\text{CuFe}_2\text{O}_4)_x$ composites ($x = 2, 3, 4,$ and 5) was performed using the Nicholson–Ross–Weer method (NRW) [37] by measuring the so called ‘scattering’ parameters of the coaxial line segment S11 and S21. Figure 7a and b demonstrate the frequency dependence of the S11–S21 parameters. These parameters correspond to the transition and reflection losses (attenuation in incident power of the radiation).

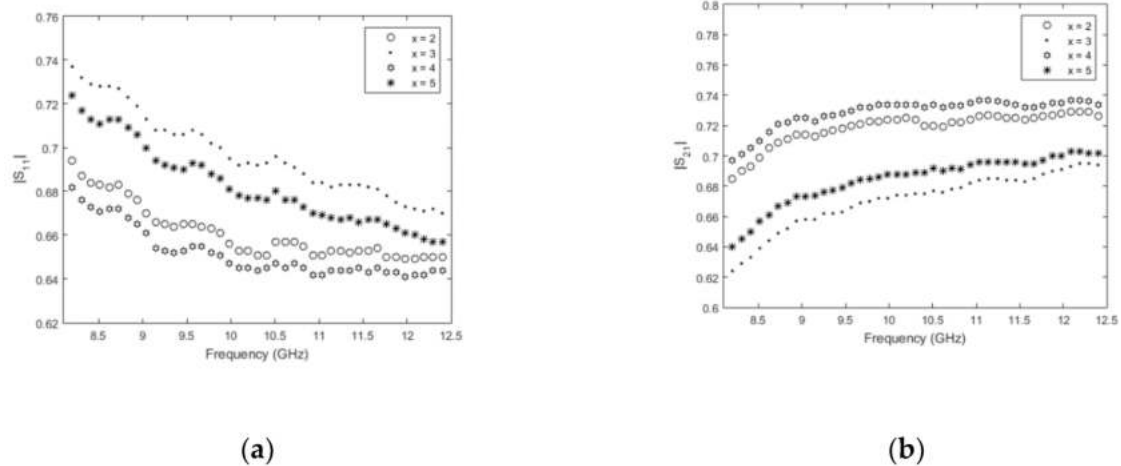


Figure 7. Frequency dependencies of (a) S11 and (b) S21 parts for $\text{Sr}_{0.3}\text{Ba}_{0.4}\text{Pb}_{0.3}\text{Fe}_{12}\text{O}_{19}/(\text{CuFe}_2\text{O}_4)_x$ composite samples ($x = 2, 3, 4$ and 5).

Figure 8 demonstrates the reflection losses (RL) for $\text{Sr}_{0.3}\text{Ba}_{0.4}\text{Pb}_{0.3}\text{Fe}_{12}\text{O}_{19}/(\text{CuFe}_2\text{O}_4)_x$ composites ($x = 2, 3, 4,$ and 5). The maximal values of RL for $x = 3$ and 5 are less than -4.5 dB thus the main losses are due to reflection rather than absorption. Using transmission (TL – transmission losses) and reflection (RL – reflection losses) coefficients, the absorption coefficient k_{abs} was calculated as follows [22]:

$$k_{abs} = 10 \log (1 - 10^{0.1k_{tr}} - 10^{0.1k_{ref}}) \quad (7)$$

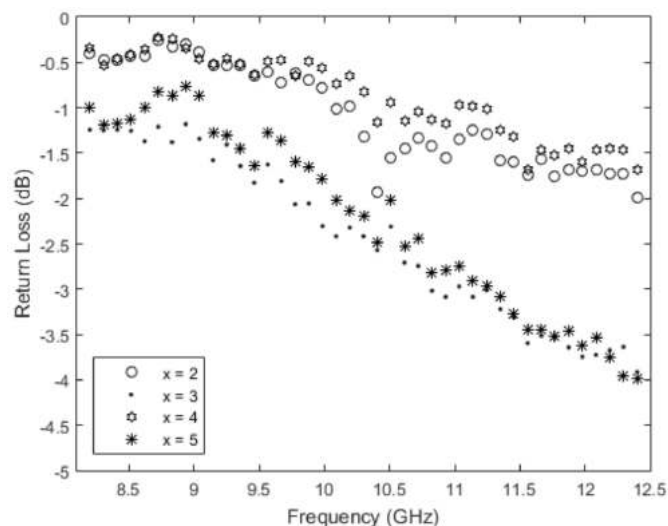


Figure 8. Frequency dependencies of reflection for $\text{Sr}_{0.3}\text{Ba}_{0.4}\text{Pb}_{0.3}\text{Fe}_{12}\text{O}_{19}/(\text{CuFe}_2\text{O}_4)_x$ composite samples ($x = 2, 3, 4$ and 5).

Figure 9 demonstrates the frequency dependence of absorption losses for the composites investigated in the frequency range 8–12 GHz. It is clear that no sufficient weakening was caused by electromagnetic absorption in this frequency range. It must be mentioned that this frequency range is

a typical region of absorption for ferrites with a hexagonal structure. It means that the mixing of hard and soft magnetic phases in composites leads to a significant decrease in the microwave properties of hexagonal ferrites (hard magnets).

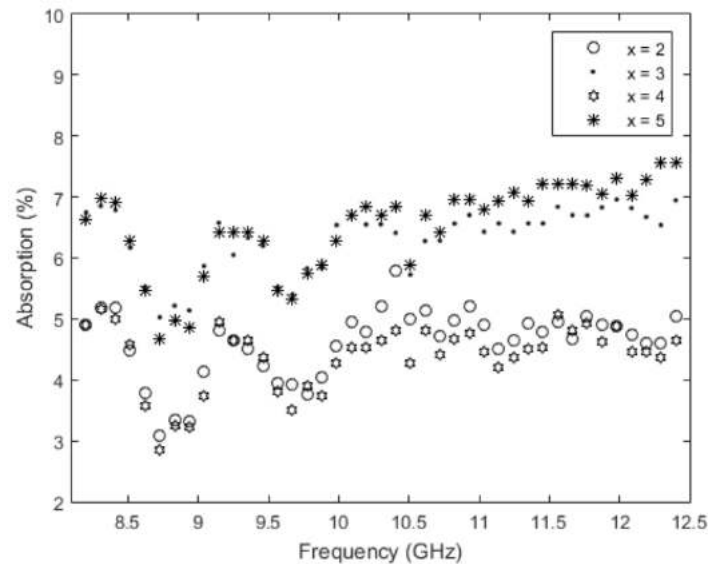


Figure 9. Frequency dependencies of absorption for $\text{Sr}_{0.3}\text{Ba}_{0.4}\text{Pb}_{0.3}\text{Fe}_{12}\text{O}_{19}/(\text{CuFe}_2\text{O}_4)_x$ composite samples ($x = 2, 3, 4$ and 5).

Figure 10 demonstrates the frequency dependence of absorption losses measured using a coaxial method in the frequency range 1 MHz–1 GHz. This frequency region was chosen due to the possibility of observing resonance reflection (NFMR) in the soft magnetic phase (spinel). It is noted that the presence of resonance (significant weakening of the reflected radiation) in this frequency range is typical of spinels [38,39]. Such behavior is due to a strong coupling between soft magnetic and hard magnetic phases that results in a weakening of the absorption for hard the magnetic phase and an increased reflection for soft magnetic phase as a function of the phase ratio concentration.

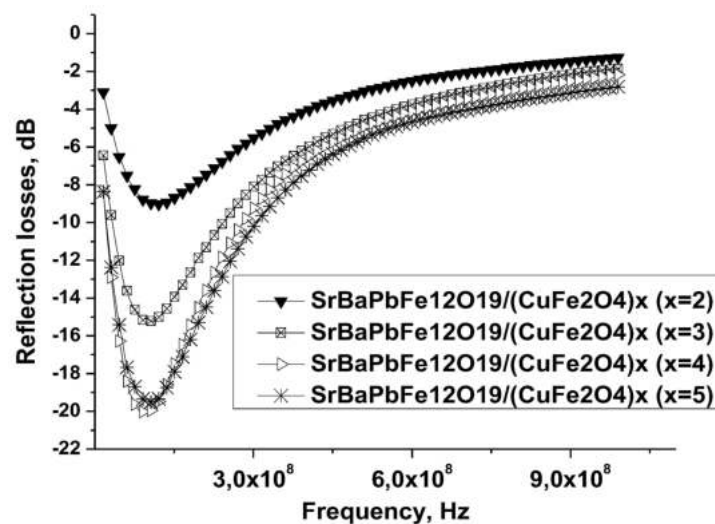


Figure 10. Frequency dependencies of the reflection losses (in dB) for $\text{Sr}_{0.3}\text{Ba}_{0.4}\text{Pb}_{0.3}\text{Fe}_{12}\text{O}_{19}/(\text{CuFe}_2\text{O}_4)_x$ composite samples ($x = 2, 3, 4$ and 5).

Figure 11 demonstrates the concentration dependence of the maximum value of reflection or resonant amplitude (A_{res}) and of the resonant frequency (F_{res}) corresponding to A_{res} . It was

demonstrated in the top graph of Figure 11 that the increase of the x value leads to an increase in the reflection losses maximum (as modulus) from -8.36 dB for $x = 1$ to -20 and -19.5 dB for $x = 4$ and $x = 5$ respectively.

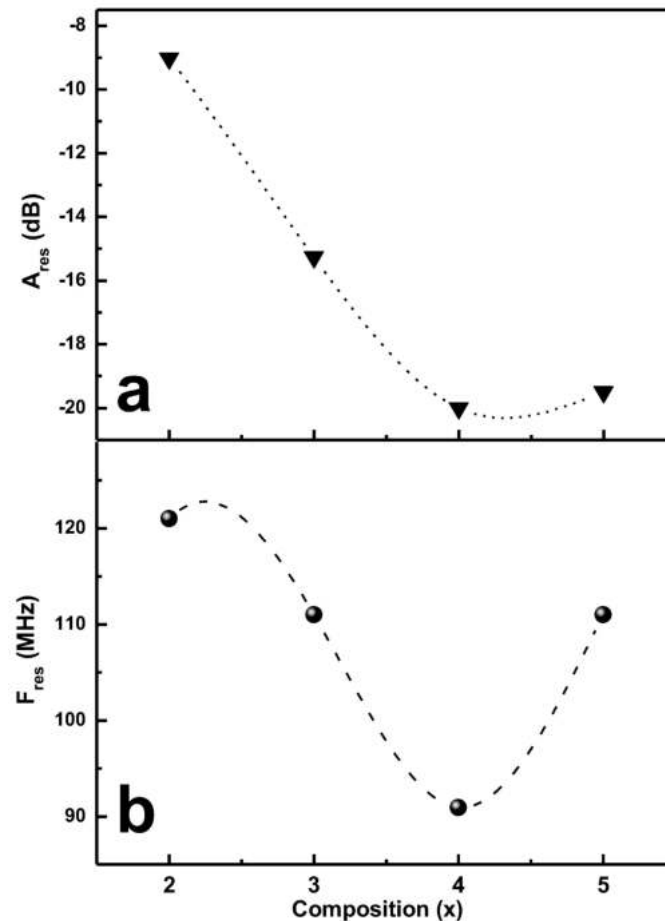


Figure 11. Composition dependencies of the resonant amplitude $-A_{res}$ (a) and resonant frequency $-F_{res}$ (b) for $Sr_{0.3}Ba_{0.4}Pb_{0.3}Fe_{12}O_{19}/(CuFe_2O_4)_x$ composite samples ($x = 2, 3, 4$ and 5).

Monotonic increase in the reflection coefficient corresponds to the resonance absorption processes. This could be due to an increase in the spinel phase in composite materials. It is well known that resonant frequency of absorption for spinels is observed in the MHz range (from several tens to several hundred MHz depending on the composition). Modification of the resonant frequency as a function of x is not linear and has complex behavior. Nevertheless, the range of F_{res} is not wide (min $F_{res} = 91$ MHz for $x = 4$ and max $F_{res} = 121$ MHz for $x = 2$). It means that absorption in investigated composites is characterized by resonant phenomena in spinel phase (for M-type hexaferrites $F_{res} \sim 50$ – 51 GHz). Non-linear shifts in F_{res} may be the result of intergranular interactions between two magnetic phases in composites.

4. Conclusions

Measurements of the MW characteristics for several typologies of nanoferrites [$Sr_{0.3}Ba_{0.4}Pb_{0.3}Fe_{12}O_{19}/(CuFe_2O_4)_x$ ($x = 2, 3, 4$, and 5)] were performed using a coaxial method in the X-band (frequency range 8–12 GHz). It was observed that differences in values of the real part of permittivity and conductivity occur depending on the ferrites compositions. This non-linear behavior may be the result of different degrees of oxidation on spinel/hexaferrite grain boundaries with a high value of the activation energy of the intergranular potential barrier. As expected in the range of 8–12 GHz, the highest RL was found for

$x = 3$ and 5 (less than -4.5 dB), meaning that the main losses are due to reflection rather than absorption. The strong coupling between phases was established by measurements performed using a coaxial method in the frequency range 1 MHz– 1 GHz. In this frequency range there was a resonance behavior which is typical for spinels. It was demonstrated that the reflection losses maximum (as modulus) increases with an increasing x value from -9.1 dB (for $x = 2$) to -20 – 19.5 dB (for $x = 4$ and $x = 5$ respectively). Monotonic increase in the reflection coefficient corresponds to the resonance absorption processes. This may be due to an increase in the spinel phase influence. Non-linear shifts in F_{res} may be the result of intergranular interaction between two magnetic phases in composites. Effective absorption of these composites opens broad perspectives for their exploitation in 4G-technology (information transfer) as well as for biomedical applications (for example, as magnetic nanoparticles for hyperthermic applications against cancer).

Author Contributions: Synthesis of the sample, writing—original draft preparation, M.A.A.; Investigation electromagnetic properties and writing, Y.S., K.Y. and F.E.; XRD investigations and analysis, M.Z.; Investigation and analysis, E.L.T., A.S., K.C.; Supervision, A.B. and A.V.T.; Review and Editing, S.V.T.

Funding: Authors are grateful to the Institute for Research and Medical Consultations (IRMC) of Imam Abdulrahman Bin Faisal University (IAU-Saudi Arabia) for the financial supports to pursue this research (Grant No: 2018-IRMC-S-1 and 2018-IRMC-S-2). This work was performed with partial financial supports from the Ministry of Education and Science of the Russian Federation in the framework of Increase Competitiveness Program of NUST «MISiS» (grants No. II02-2017-2-4, No. K4-2017-041 and No. K3-2018-026) and SUSU (grant No. 4.1346.2017/4.6).

Acknowledgments: The technical assistance provided by Core Labs of King Abdullah University of Science and Technology (KAUST) are highly appreciated.

Conflicts of Interest: The authors declare no conflicts of interest.

References

1. Tokunaga, Y.; Kaneko, Y.; Okuyama, D.; Ishiwata, S.; Arima, T.; Wakimoto, S.; Kakurai, K.; Taguchi, Y.; Tokura, Y. Multiferroic M-Type Hexaferrites with a Room-Temperature Conical State and Magnetically Controllable Spin Helicity. *Phys. Rev. Lett.* **2010**, *105*, 257201. [[CrossRef](#)] [[PubMed](#)]
2. Lin, Q.; Xu, J.; Yang, F.; Lin, J.; Yang, H.; He, Y. Magnetic and Mössbauer Spectroscopy Studies of Zinc-Substituted Cobalt Ferrites Prepared by the Sol-Gel Method. *Materials* **2018**, *11*, 1799. [[CrossRef](#)] [[PubMed](#)]
3. Kumar, A.; Agarwala, V.; Singh, D. Effect of particle size of BaFe₁₂O₁₉ on the microwave absorption characteristics in X-band. *Prog. Electromagn. Res.* **2013**, *M29*, 223–236. [[CrossRef](#)]
4. Yajima, T. Titanium Pnictide Oxide Superconductors. *Condens. Matter* **2017**, *2*, 4. [[CrossRef](#)]
5. Demokritov, S.O.; Demidov, V.E.; Dzyapko, O.; Melkov, G.A.; Serga, A.A.; Hillebrands, B.; Slavin, A.N. Bose–Einstein condensation of quasi-equilibrium magnons at room temperature under pumping. *Nature* **2006**, *443*, 430–433. [[CrossRef](#)] [[PubMed](#)]
6. Kostishyn, V.G.; Panina, L.V.; Timofeev, A.V.; Kozhitov, L.V.; Kovalev, A.N.; Zyuzin, A.K. Dual ferroic properties of hexagonal ferrite ceramics BaFe₁₂O₁₉ and SrFe₁₂O₁₉. *J. Magn. Magn. Mater.* **2016**, *400*, 327–332. [[CrossRef](#)]
7. Trukhanov, S.V.; Trukhanov, A.V.; Kostishin, V.G.; Panina, L.V.; Kazakevich, I.S.; Turchenko, V.A.; Kochervinskiy, V.V. Coexistence of spontaneous polarization and magnetization in substituted M-type hexaferrites BaFe_{12-x}Al_xO₁₉ ($x \leq 1.2$) at room Temperature. *JETP Lett.* **2016**, *103*, 100–105. [[CrossRef](#)]
8. Wang, P.; Xiang, H. Room-temperature ferrimagnet with frustrated antiferroelectricity: Promising candidate toward multiple-state memory. *Phys. Rev. X* **2014**, *4*, 011035. [[CrossRef](#)]
9. Nan, C.W.; Bichurin, M.I.; Dong, S.; Viehland, D.; Srinivasan, G. Multiferroic magnetoelectric composites: Historical perspective, status, and future directions. *J. Appl. Phys.* **2008**, *103*, 031101. [[CrossRef](#)]
10. Liu, G.; Nan, C.W.; Xu, Z.K.; Chen, H.D. Coupling interaction in multiferroic BaTiO₃-CoFe₂O₄ nanostructures. *J. Phys. D Appl. Phys.* **2005**, *38*, 2321–2326. [[CrossRef](#)]
11. Zhang, H.F.; Or, S.W.; Chan, H.L.W. Multiferroic properties of Ni_{0.5}Zn_{0.5}Fe₂O₄-Pb(Zr_{0.53}Ti_{0.47})O₃ ceramic composites. *J. Appl. Phys.* **2008**, *104*, 104109. [[CrossRef](#)]

12. Trukhanov, S.V.; Trukhanov, A.V.; Salem, M.M.; Trukhanova, E.L.; Panina, L.V.; Kostishyn, V.G.; Darwish, M.A.; Trukhanov, A.V.; Zubar, T.I.; Tishkevich, D.I.; et al. Preparation and investigation of structure, magnetic and dielectric properties of $(\text{BaFe}_{11.9}\text{Al}_{0.1}\text{O}_{19})_{1-x}-(\text{BaTiO}_3)_x$ bicomponent ceramics. *Ceram. Int.* **2018**, *44*, 21295–21302. [[CrossRef](#)]
13. Turchenko, V.; Trukhanov, A.; Trukhanov, S.; Bobrikov, I.; Balagurov, A. Features of crystal and magnetic structures of solid solutions $\text{Ba}_{12-x}\text{D}_x\text{O}_{19}$ ($\text{D}=\text{Al}^{3+}, \text{In}^{3+}; x=0.1$) in a wide temperature range. *Eur. Phys. J. Plus* **2016**, *131*, 82–89. [[CrossRef](#)]
14. Pastore, R.; Delfini, A.; Micheli, D.; Vricella, A.; Marchetti, M.; Santoni, F.; Piergentili, F. Carbon foam electromagnetic mm-wave absorption in reverberation chamber. *Carbon* **2019**, *144*, 63–71. [[CrossRef](#)]
15. Mazzoli, A.; Corinaldesi, V.; Donnini, J.; di Perna, C.; Micheli, D.; Vricella, A.; Pastore, R.; Bastianelli, L.; Moglie, F.; Primiani, V.M. Effect of graphene oxide and metallic fibers on the electromagnetic shielding effect of engineered cementitious composites. *J. Build. Eng.* **2018**, *18*, 33–39. [[CrossRef](#)]
16. Micheli, D.; Pastore, R.; Vricella, A.; Marchetti, M. Matter's electromagnetic signature reproduction by graded-dielectric multilayer assembly. *IEEE Trans. Microw. Theory Techn.* **2017**, *5*, 2801–2809. [[CrossRef](#)]
17. Micheli, D.; Vricella, A.; Pastore, R.; Marchetti, M. Synthesis and electromagnetic characterization of frequency selective radar absorbing materials using carbon nanopowders. *Carbon* **2014**, *77*, 756–774. [[CrossRef](#)]
18. Kuświk, P.; Gaul, A.; Urbaniak, M.; Schmidt, M.; Aleksiejew, J.; Ehresmann, A.; Stobiecki, F. Tailoring Perpendicular Exchange Bias Coupling in Au/Co/NiO Systems by Ion Bombardment. *Nanomaterials* **2018**, *8*, 813. [[CrossRef](#)]
19. Chen, Y.-T.; Lin, S.-H.; Sheu, T.-S. Effect of Low-Frequency AC Magnetic Susceptibility and Magnetic Properties of CoFeB/MgO/CoFeB Magnetic Tunnel Junctions. *Nanomaterials* **2014**, *4*, 46–54. [[CrossRef](#)]
20. Yang, H.; Ye, T.; Lin, Y.; Liu, M. Exchange coupling behavior and microwave absorbing property of the hard/soft $(\text{BaFe}_{12}\text{O}_{19}/\text{Y}_3\text{Fe}_5\text{O}_{12})$ ferrites based on polyaniline. *Synth. Metals* **2015**, *210*, 245–250. [[CrossRef](#)]
21. Trukhanov, S.V.; Trukhanov, A.V.; Kostishyn, V.G.; Panin, L.V.; Trukhanov, A.V.; Turchenko, V.A.; Tishkevich, D.I.; Trukhanova, E.L.; Oleynik, V.V.; Yakovenko, E.S.; et al. Magnetic, dielectric and microwave properties of the $\text{BaFe}_{12-x}\text{GaxO}_{19}$ ($x \leq 1.2$) solid solutions at room temperature. *J. Magn. Magn. Mater.* **2017**, *442*, 300–310. [[CrossRef](#)]
22. Trukhanov, S.V.; Trukhanov, A.V.; Kostishyn, V.G.; Panina, L.V.; Trukhanov, A.V.; Turchenko, V.A.; Tishkevich, D.I.; Trukhanova, E.L.; Yakovenko, E.S.; Matzui, L.Y. Investigation of structure features and microwave absorption by doped barium hexaferrites. *Dalton Trans.* **2017**, *46*, 9010–9021. [[CrossRef](#)] [[PubMed](#)]
23. Skomski, R.; Coey, J.M.D. Giant energy product in nanostructured two-phase magnets. *Phys. Rev. B* **1993**, *48*, 15812. [[CrossRef](#)]
24. Feng, C.; Liu, X.G.; Siu, W.O.; Ho, S.L. Exchange coupling and microwave absorption in core/shell-structured hard/soft ferrite-based $\text{CoFe}_2\text{O}_4/\text{NiFe}_2\text{O}_4$ nanocapsules. *AIP Adv.* **2017**, *7*, 056403. [[CrossRef](#)]
25. Afshar, S.R.S.; Hasheminasari, M.; Masoudpanah, S.M. Structural, magnetic and microwave absorption properties of $\text{SrFe}_{12}\text{O}_{19}/\text{Ni}_{0.6}\text{Zn}_{0.4}\text{Fe}_2\text{O}_4$ composites prepared by one-pot solution combustion method. *J. Magn. Magn. Mater.* **2018**, *466*, 1–6. [[CrossRef](#)]
26. Shen, X.Q.; Song, F.Z.; Xiang, J.; Liu, M.Q.; Zhu, Y.W.; Wang, Y.D. Shape Anisotropy, Exchange-Coupling Interaction and Microwave Absorption of Hard/Soft Nanocomposite Ferrite Microfibers. *J. Am. Ceram. Soc.* **2012**, *95*, 3863–3870. [[CrossRef](#)]
27. Torkian, S.; Ghasemi, A.; Razavi, R.S. Magnetic properties of hard-soft $\text{SrFe}_{10}\text{Al}_2\text{O}_{19}/\text{Co}_{0.8}\text{Ni}_{0.2}\text{Fe}_2\text{O}_4$ ferrite synthesized by one-pot sol-gel autocombustion. *J. Magn. Magn. Mater.* **2016**, *416*, 408–416. [[CrossRef](#)]
28. Bennet, J.; Tholkappian, R.; Vishista, K. Attestation in self-propagating combustion approach of spinel AFe_2O_4 ($\text{A}=\text{Co}, \text{Mg}$ and Mn) complexes bearing mixed oxidation states: Magnetostructural properties. *Appl. Surf. Sci.* **2016**, *383*, 113–125. [[CrossRef](#)]
29. Han, Q.; Meng, X.; Lu, C. Exchange-coupled $\text{Ni}_{0.5}\text{Zn}_{0.5}\text{Fe}_2\text{O}_4/\text{SrFe}_{12}\text{O}_{19}$ composites with enhanced microwave absorption performance. *J. Alloys Compd.* **2018**, *768*, 742–749. [[CrossRef](#)]
30. Almessiere, M.A.; Slimani, Y.; Baykal, A. Exchange spring magnetic behavior of $\text{Sr}_{0.3}\text{Ba}_{0.4}\text{Pb}_{0.3}\text{Fe}_{12}\text{O}_{19}/(\text{CuFe}_2\text{O}_4)_x$ nanocomposites fabricated by a one-pot citrate sol-gel combustion method. *J. Alloys Compd.* **2018**, *762*, 389–397. [[CrossRef](#)]

31. Klygach, D.S.; Vakhitova, M.G.; Vinnik, D.A.; Bezborodov, A.V.; Gudkova, S.A.; Zhivulin, V.E.; Zherebtsov, D.A.; Trukhanov, S.V.; Trukhanov, A.V.; Starikov, A.Y. Measurement of permittivity and permeability of barium hexaferrite. *J. Magn. Magn. Mater.* **2018**, *456*, 290–294. [[CrossRef](#)]
32. Vinnik, D.A.; Klygach, D.S.; Zhivulin, V.E.; Malkin, A.I.; Vakhitov, M.G.; Gudkova, S.A.; Galimov, D.M.; Zherebtsov, D.A.; Trofimov, E.A.; Knyazev, N.S.; et al. Electromagnetic properties of BaFe₁₂O₁₉:Ti at centimeter wavelengths. *J. Alloys Compd.* **2018**, *755*, 177–183. [[CrossRef](#)]
33. Trukhanov, A.V.; Trukhanov, S.V.; Kostishyn, V.G.; Panina, L.V.; Korovushkin, V.V.; Turchenko, V.A.; Vinnik, D.A.; Yakovenko, E.S.; Zagorodnii, V.V.; Launetz, V.L.; et al. Correlation of the atomic structure, magnetic properties and microwave characteristics in substituted hexagonal ferrites. *J. Magn. Magn. Mater.* **2018**, *462*, 127–135. [[CrossRef](#)]
34. Trukhanov, A.V.; Kostishyn, V.G.; Panina, L.V.; Korovushkin, V.V.; Turchenko, V.A.; Thakur, P.; Thakur, A.; Yang, Y.; Vinnik, D.A.; Yakovenko, E.S.; et al. Control of Electromagnetic properties in Substituted M-type Hexagonal ferrites. *J. Alloys Compd.* **2018**, *754*, 247–256. [[CrossRef](#)]
35. Trukhanov, A.V.; Panina, L.V.; Trukhanov, S.V.; Kostishyn, V.G.; Turchenko, V.A.; Vinnik, D.A.; Zubar, T.I.; Yakovenko, E.S.; Macuy, L.Y.; Trukhanova, E.L. Critical Influence of Different Diamagnetic Ions on Electromagnetic Properties of BaFe₁₂O₁₉. *Ceram. Int.* **2018**, *44*, 13520–13529. [[CrossRef](#)]
36. Tong, L.; Zha, H.; Tian, Y. Determining the complex permittivity of powder materials from 1–40 GHz using transmission-line technique. In Proceedings of the IEEE International Geoscience and Remote Sensing Symposium, Melbourne, VIC, Australia, 21–26 July 2013; pp. 1380–1382.
37. Nicolson, A.M.; Ross, G.F. Measurement of the intrinsic properties of materials by time-domain techniques. *IEEE Trans. Instrum. Meas.* **1970**, *19*, 77–382. [[CrossRef](#)]
38. Wang, W.; Jiao, Q.; Zang, C.; Zhu, X. Study on the Absorption Properties of Spinel Type Ferrite Composite Coatings in the Low Frequency. *Adv. Mater. Res.* **2011**, *415–417*, 30–34. [[CrossRef](#)]
39. Stergiou, C. Magnetic, dielectric and microwave absorption properties of rare earth doped Ni–Co and Ni–Co–Zn spinel ferrites. *J. Magn. Magn. Mater.* **2017**, *426*, 629–635. [[CrossRef](#)]



© 2019 by the authors. Licensee MDPI, Basel, Switzerland. This article is an open access article distributed under the terms and conditions of the Creative Commons Attribution (CC BY) license (<http://creativecommons.org/licenses/by/4.0/>).